Real-Time Phosphate Sensing in Living Cells using Fluorescence Lifetime Imaging Microscopy (FLIM)

ARTICLE *in* THE JOURNAL OF PHYSICAL CHEMISTRY B · JUNE 2013

Impact Factor: 3.3 · DOI: 10.1021/jp405041c · Source: PubMed

8 AUTHORS, INCLUDING:

Maria J Ruedas-Rama
University of Granada
38 PUBLICATIONS **685** CITATIONS
SEE PROFILE

Angel Orte
University of Granada
66 PUBLICATIONS **1,181** CITATIONS
SEE PROFILE

Rafael Salto
University of Granada
53 PUBLICATIONS **905** CITATIONS
SEE PROFILE

Jose M Alvarez-Pez
University of Granada
63 PUBLICATIONS **918** CITATIONS
SEE PROFILE

THE JOURNAL OF PHYSICAL CHEMISTRY B

Article

pubs.acs.org/JPCB

Real-Time Phosphate Sensing in Living Cells using Fluorescence Lifetime Imaging Microscopy (FLIM)

Jose M. Paredes,[†] Maria D. Giron,[‡] Maria J. Ruedas-Rama,[†] Angel Orte,[†] Luis Crovetto,[†] Eva M. Talavera,[†] Rafael Salto,[‡] and Jose M. Alvarez-Pez*[,†]

[†]Department of Physical Chemistry and [‡]Department of Biochemistry and Molecular Biology, University of Granada

Supporting Information

ABSTRACT: Phosphate ions play important roles in signal transduction and energy storage in biological systems. However, robust chemical sensors capable of real-time quantification of phosphate anions in live cells have not been developed. The fluorescein derivative dye 9-[1-(2-methyl-4-methoxyphenyl)]-6-hydroxy-3H-xanthen-3-one (2-Me-4-OMe TG) exhibits the characteristic excited-state proton-transfer (ESPT) reaction of xanthenic derivatives at approximately physiological pH resulting in the dependence of the dye's nanosecond fluorescence decay time on the phosphate buffer concentration. This allows the 2-Me-4-OMe TG dye to be used with fluorescence lifetime imaging microscopy (FLIM) as a real-time phosphate intracellular sensor in cultured cells. This methodology has allowed the time course of cellular differentiation of MC3T3-E1 murine preosteoblast cells to be measured on the basis of the decrease in the decay time of 2-Me-4-OMe TG. These changes were consistent with increased alkaline phosphatase activity in the extracellular medium as a marker of the differentiation process.

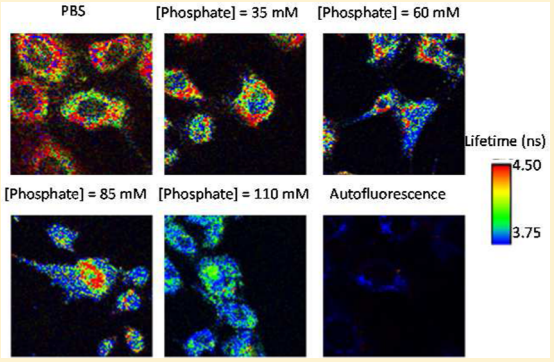

INTRODUCTION

Monitoring changes in the concentrations of biologically important anions inside living cells has attracted attention in the development of new analytical techniques. Although anions are generally more difficult to detect, sensors based on anion-induced changes in fluorescent parameters are particularly attractive because of their noninvasive character and low detection limit. Fluorescence lifetime imaging microscopy (FLIM)[1] is an effective technique for quantitative real-time sensing of biologically important targets inside living cells[2−4] since FLIM is an excellent alternative to fluorescence intensity and fluorescence ratiometric measurements because it is concentration independent and because only a single excitation wavelength/emission interval is required.[5]

The recognition and sensing of phosphate ions is a popular research topic. Phosphate anions play important roles in signal transduction and energy storage in biological systems. Signal transduction is mainly based on the transfer of phosphate groups to regulatory proteins. Phosphorylation status is regulated by protein kinases and phosphatases.[6] Accordingly, the detection of an increase or decrease in the phosphate concentration in the environment of these enzymes is a common method for monitoring enzyme activity or the protein phosphorylation process.[7] Phosphate is also involved in bone mineralization. Inside the osteoblast, phosphate functions as an important constituent of the bone minerals and an important signaling molecule. Increases in intracellular phosphate trigger a series of cellular and molecular changes that prepare the cell and the extracellular matrix for a mineralization competent state.[8] Therefore, the detection and quantification of phosphate inside the cell and in the extracellular media is relevant in the study of the process of bone mineralization. The development of fluorescent sensors for measuring phosphate under aqueous physiological conditions is challenging because of strong hydration effects.[9] Beyond invasive approaches employing radioactive phosphate, which are associated with several drawbacks,[10] there are a few chemical sensors capable of detecting phosphate anions in an aqueous physiological system,[11] but none of them is able to estimate the real-time concentration of phosphate inside live cells.

The challenges of measuring phosphate in cells have motivated us to develop real-time fluorescent sensors for detecting intracellular levels of phosphate. The sensor proposed herein is based on an excited-state proton-transfer (ESPT) reaction characteristic of xanthenic fluorescein derivatives. Fluorescein is a complex fluorescent molecule with several prototropic forms in aqueous solution. At approximately physiological pH, only the monoanion/dianion equilibrium is relevant. Fluorescein undergoes an ESPT reaction, which interconverts the mono- and dianion forms in the presence of a suitable proton donor−acceptor at near neutral pH and which strongly alters the fluorescence emission signal.[12] In particular, the ionic species of phosphate act as suitable proton donors and acceptors to promote the ESPT reaction at the physiological

Received: May 22, 2013
Revised: June 12, 2013
Published: June 13, 2013

   dx.doi.org/10.1021/jp405041c | J. Phys. Chem. B 2013, 117, 8143−8149

pH.[12,13] By recording fluorescence decay traces and using powerful analytical methods, the specific rate constants of the ESPT reactions have been evaluated.[14,15] Using these rate constants values, the steady-state fluorescence intensity and fluorescence decay time values may be calculated at any pH and phosphate concentration.[13,16] Moreover, the presence of other ions, not involved in the proton-transfer reaction, has a negligible effect on the fluorescence decay times.[17]

These reactions are characteristic of other xanthenic derivatives in addition to fluorescein,[18,19] and the presence of these excited-state reactions influences the decay traces from excited fluorescein derivatives and causes the decay times to vary depending on both the pH and the phosphate concentration. However, the biexponential character of the fluorescence decay limits the use of fluorescent dyes in FLIM sensing.[20,21] An improved sensor dye for FLIM would exhibit monoexponential fluorescence decays with a lifetime dependent on the sensed experimental parameters (e.g., solvent pH or buffer concentration). For this reason, our interest was to find fluorescein derivatives capable of undergoing the characteristic phosphate-mediated ESPT reaction with a monoexponential decay time in the near-neutral pH region. We observed these desirable features in two dyes: 9-[1-(2-methoxy-5-methylphenyl)]-6-hydroxy-3H-xanthen-3-one (2-OMe-5-Me TG)[22] and 9-[1-(2-methyl-4-methoxyphenyl)]-6-hydroxy-3H-xanthen-3-one (2-Me-4-OMe TG),[23] which are two xanthenic derivatives of the Tokyo Green dye family.[24] These two dyes undergo a characteristic ESPT reaction in which the fluorescence from the prototropic forms exhibits a phosphate-sensitive decay time on the order of nanoseconds, while the other decay times are on the order of subnanoseconds.[22,23]

In this work, we evaluated the ability of 2-Me-4-OMe TG (see Scheme 1) for measuring the changes in the intracellular phosphate concentration using FLIM. We chose 2-Me-4-OMe TG instead of 2-OMe-5-Me TG because of the higher quantum yield of the former. To do this, the longest decay time from the characteristic ESPT reaction of the dye was employed to estimate the changes in the intracellular phosphate levels upon permeabilization of the cell membrane. The excellent agreement between the changes in the fluorescence decay time from the dye inside the cells and the changes in the extracellular concentration of phosphate encouraged us to test the ability of 2-Me-4-OMe TG as a sensor of phosphate inside MC3T3-E1 murine preosteoblast cell line, which is a well-established model for osteoblast differentiation.[25] Thus, we were able to assess the transport of extracellular phosphate into preosteoblasts during osteoblast differentiation recovering the apparent kinetic rate constant of incorporation of phosphate into the cellular cytoplasm. Our results showed that the intracellular levels of phosphate, as evidenced by the decrease in the decay time of the dye, correlated with the extracellular activity of alkaline phosphatase. CHO-k1 cells, which lack the phosphate transport system, were employed as a negative control.

Scheme 1. Chemical Structures and Proton Exchange Reaction of 2-Me-4-OMe TG Forms at Near-Neutral pH: 1, Neutral; 2, Anion[a]

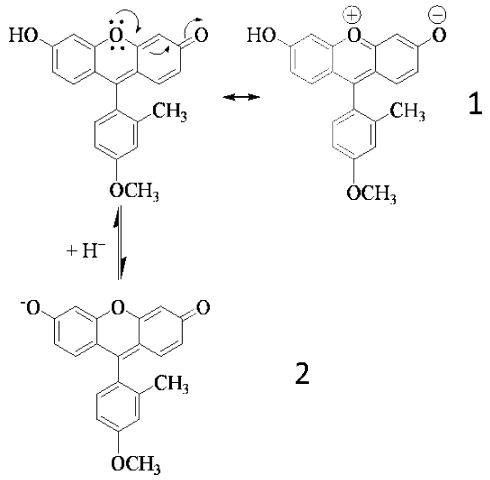

[a]The neutral form is represented by two resonance structures.

EXPERIMENTAL SECTION

Materials and Solutions. Dulbecco's modified Eagle's medium (DMEM, D-6546), α-minimum essential medium (α-MEM), fetal bovine serum (FBS), penicillin/streptomycin, trypsin-EDTA, α-hemolysin from *Staphylococcus aureus*, ascorbic acid, and β-glycerol phosphate were obtained from Sigma Chemical (St. Louis, MO). All other reagents were analytical grade. The fluorescent dye 9-[1-(2-methyl-4-methoxyphenyl)]-6-hydroxy-3H-xanthen-3-one (2-Me-4-OMe TG) was prepared as described in the literature.[23] Stock solutions of sodium phosphate were prepared using $NaH_2PO_4 \times H_2O$ and $Na_2HPO_4 \times 7H_2O$ (both Fluka, puriss. p.a.) in appropriate amounts to obtain the required pH. Commercially available phosphate-buffered saline (PBS) (Sigma-Aldrich) was also used. To obtain the required phosphate concentration in the measurement solutions, the necessary amount of phosphate stock solution was added to PBS and DMEM. Trizma (Sigma, puriss. p.a.) was used to maintain the DMEM pH. Spectroscopic-grade NaOH (Aldrich, platelets) was used to adjust the pH of the buffer.

All solutions were prepared using Milli-Q water as the solvent. Solutions without proteins were filtered through 0.02 μm filters (Whatman) before use. All chemicals were used as received without further purification. Solutions were kept cool in the dark when not in use to avoid possible deterioration by light and heat. Aliquots of α-toxin from *Staphylococcus aureus* were prepared and were stored in a freezer (−20 °C) until use.

Cell Culture. Wild-type Chinese hamster ovary (CHO-k1; ATCC No. CCL-61) and MC3T3-E1 preosteoblast (ECACC 99072810) cell lines were provided by the Cell Culture Facility, University of Granada. CHO-k1 cells were grown in Dulbecco's modified Eagle's medium (DMEM) supplemented with 10% (v/v) FBS, 2 mM glutamine, 100 U/mL penicillin, and 0.1 μg/mL streptomycin in a humidified 5% CO_2 incubator. MC3T3-E1 cells were grown in alpha minimum essential medium (αMEM) containing 10% fetal bovine serum and 1% penicillin−streptomycin in a humidified 5% CO_2 incubator as described previously.[25] For the osteoblast differentiation time course experiments, MC3T-E1 cells were grown for up to 6 days. At time 0, cells at 90% confluence were grown in αMEM containing 10% fetal bovine serum supplemented with 3 mM phosphate, 50 μg/μL ascorbic acid (AA) (a critical cofactor required for collagen production), and 10 mM β-glycerophosphate (βGP), and the cells were analyzed at the indicated times.

For the FLIM microscopy experiments, CHO-k1 and MC3T3-E1 cells were seeded onto 20 mm coverslips in 12 well plates at a density of 11 250 cells/cm^2. The coverslips were translated to the MicroTime 200 fluorescence lifetime micro-

dx.doi.org/10.1021/jp405041c | J. Phys. Chem. B 2013, 117, 8143−8149

scope system (see below) and were washed with PBS before adding work solutions.

Cell Permeabilization. CHO-K1 and MC3T3-E1 cells were deposited onto coverslips in 12 well plates and were incubated with their respective media. On the day of the experiment, the cells were washed twice with phosphate-buffered saline (PBS) and were perforated by incubation for 15 min at 37 °C with 2 μg/mL α-toxin in permeabilization buffer (20 mM potassium MOPS, pH 7.0, 250 mM mannitol, 1 mM potassium ATP, 3 mM $MgCl_2$, and 5 mM potassium glutathione).[26] Afterward, the cells were washed twice with PBS and were analyzed by FLIM.

Phosphatase Alkaline Measurement. Phosphatase alkaline activity was measured in the incubation media of MC3T3-E1 cells using a spectrophotometric method on the basis of the hydrolysis of p-nitrophenylphosphate following the kit instructions (Spinreact, Barcelona, Spain).

Ensemble Time-Resolved Fluorescence Instrumentation. Fluorescence decay traces at the ensemble level were recorded using the time-correlated single photon timing (TCSPT)[1,27] method with a FluoTime 200 fluorometer (PicoQuant, Inc., Germany). The excitation source consisted of an LDH-485 pulsed laser with a minimum pulse width of 88 ps. The pulse repetition rate was 20 MHz. The laser pulse was directed to the solution sample in 10 × 10 mm cuvettes. The lens-focused fluorescence emission passed through a detection polarizer set at the magic angle and a detection monochromator prior to the photomultiplier detector. The fluorescence decay histograms were collected in 1320 channels with a time increment of 36 ps/channel. Histograms of the instrument response functions (using LUDOX scatter) and sample decays were recorded until they reached approximately 2×10^4 counts in the peak channel.

FLIM Instrumentation. Fluorescence lifetime images were recorded with a MicroTime 200 fluorescence lifetime microscope system (PicoQuant, Inc.) and the time-tagged time-resolved (TTTR) methodology, which permits fluorescence decay histograms to be reconstructed from molecules in the confocal volume. The excitation source consisted of the LDH 485 nm pulsed laser described previously. The light beam was directed onto a dichroic mirror (510dcxr) to the oil immersion objective (1.4 NA, 100×) of an inverted microscope system IX-71 (Olympus). The collected fluorescence light was filtered by a long-pass filter HP500LP (AHF/Chroma) and was focused onto a 75 μm confocal aperture. After the aperture, the transmitted light was refocused onto two single photon avalanche diodes SPCM-AQR 14 (Perkin-Elmer) after the signal was separated by a 50/50 beam splitter. The data acquisition was performed with a TimeHarp 200 TCSPT module (PicoQuant, Inc.) in TTTR mode, which enabled the reconstruction of the lifetime histogram. Raw images were recorded by raster scanning an area of 80 × 80 μm with a resolution of 512 × 512 pixels. The photons of each pixel were temporally sorted with respect to the excitation pulse in the histograms with a time resolution of 29 ps/channel.

The same setup was employed for collecting fluorescence decay traces of the dyes at the single molecule level. Fluorescence fluctuation traces were collected with the excitation laser focused on a single point. Dye aqueous solutions were deposited on microscope slides with a total dye concentration of less than 1 nM.

Fluorescence Decay Trace Analysis. The fluorescence decay traces at the ensemble and single-molecule levels were individually analyzed using an iterative deconvolution method with exponential models using FluoFit software (PicoQuant).

FLIM Image Analysis. The FLIM image data were analyzed using SymphoTime software (PicoQuant). To obtain the fitted FLIM images, a reconstructed instrument response function was employed to analyze the fluorescence decay histogram of each pixel within the whole image using a biexponential model. A short decay time of 1.5 ns was fixed to account for the short-lived autofluorescence of the cell, whereas the second decay time was a freely adjustable parameter. All decay histograms were fitted by applying the maximum likelihood estimator (MLE), which yields correct parameter sets for low count rates.[28] Binning of 5 × 5 pixels and prehistogramming of four temporal channels (for a final resolution of 116 ps/channel) were used to achieve a larger number of counts in each pixel.

Fluorescence Decay Histogram Reconstruction from FLIM Images and Fitting. Once the FLIM images were obtained, the pixels in the region of interest (cellular cytoplasm) were selected, and a total fluorescence decay histogram of the region of interest was reconstructed. To obtain a single, average lifetime value from the dye in the intracellular cytoplasm, the fluorescence decay traces were fitted using a tailfit method with a time gate of 1.5 ns after the excitation pulse. A biexponential model was employed using a fixed short decay time of 1.5 ns (lifetime arising from the interaction between the dye and the intracellular components) and a freely adjustable long decay time (tuning lifetime, sensitive to phosphate concentration). The value of the long decay time is reported in Figures 2−5.

RESULTS AND DISCUSSION

The theory of buffer-mediated ESPT reactions is well established, and details on global bicompartmental analysis and the determination of kinetic rate constants are available.[14,15,18,19,22,23] Considering an intermolecular system (Scheme S-1 of the Supporting Information, SI) consisting of two different prototropic forms of a ground-state dye and the two corresponding excited-state species, we have shown that the ESPT reaction becomes reversible at near-neutral pH upon addition of phosphate buffer inducing a pH-dependent change in the fluorescence decay times. Importantly, the fluorescence decay of 2-Me-4-OMe TG becomes approximately mono-exponential (one of the decay times is on the order of picoseconds) at pH values higher than 6.10 and at any phosphate buffer concentration.[23] Figure 1 shows the recovered long decay time at both the ensemble and the single molecule levels at three pH values versus phosphate buffer concentration as well as the decay time calculated using the theoretical equations from the kinetic model and the rate constants estimated using a global compartmental analysis (GCA).[23] The correspondence of the simulated curve with the decay times obtained under two different fluorescence methodologies and the sensitivity toward the phosphate buffer concentration establish 2-Me-4-OMe TG as an appropriate dye for screening the chemical concentration of phosphate in single-molecule experiments at the physiological pH.

To test the capability of the 2-Me-4-OMe TG dye to estimate the concentration of phosphate in samples simulating the intracellular environment, we employed dilutions (1:5) of a commercial solution of Dulbecco's modified Eagle's medium containing inorganic salts, amino acids, vitamins, glucose, and other cell components (DMEM) in 50 mM TRIS buffer at pH 7.35 with different concentrations of phosphate ranging from

dx.doi.org/10.1021/jp405041c | J. Phys. Chem. B 2013, 117, 8143−8149

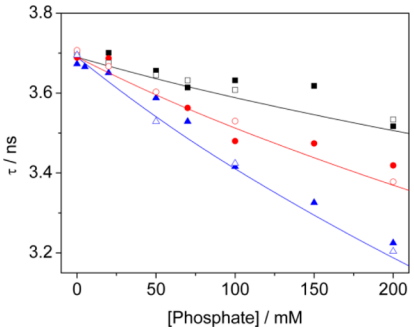

Figure 1. The decay times of 2-Me-4-OMe TG (1×10^{-7} M) at different pH values (black squares, 7.35; red circles, 7.00; and blue triangles, 6.60) recovered at the ensemble (open) and the single-molecule (filled) levels versus phosphate buffer concentration. The lines represent the simulated decay times calculated using the previously published rate constant values, which were estimated by global compartmental analysis.

10 to 210 mM. The dye was added at a concentration of 1×10^{-7} M. To construct the FLIM image, a biexponential function model was used in the deconvolution analyses of the fluorescence decay histograms in each pixel. To obtain an average value for the fluorophore decay time, the overall histograms were tail-fitted as detailed in the Experimental Section by setting a time cutoff of 1.50 ns after the excitation pulse to eliminate the background signal from the shorter decay time of the probe and medium autofluorescence. Figure S-1 of the SI shows the change in the decay time of 2-Me-4-OMe TG in the solutions. In Figure 2, the FLIM images from the samples are shown after applying an arbitrary color scale to the recovered fluorescence decay times. Considering the complexity of the matrix, the results are acceptable, and the difference in the phosphate concentration in the medium is clearly observable in the recovered images.

To gain more insight into the temporal behavior of the 2-Me-4-OMe TG fluorescence emission in the intracellular medium and the effect of different concentrations of phosphate ions, we used CHO-k1 cells. Because these cells lack a specific phosphate transport system, we compared the results for normal cells and cells that were permeabilized with α-toxin. Treatment with α-toxin generated 1.5 nm membrane pores, which permitted the diffusion of low molecular weight compounds, including both 2-Me-4-OMe TG and phosphate anions, without the loss of cytosolic proteins and high molecular weight compounds.[26] FLIM images were recorded and analyzed using the procedure described in the Experimental Section. Figure S-2 of the SI shows the changes in the fluorescence decay times of the 2-Me-4-OMe TG dye versus the phosphate concentration in both the extracellular and the intracellular media of untreated cells or cells treated with α-toxin. The changes in the theoretical values of the fluorescence decay time that should result from the different phosphate concentrations tested are also included in Figure S-2 of the SI. In the extracellular environment, the absolute values of the recovered decay times were similar to the values predicted by the kinetic model. In the nonpermeabilized CHO-k1, although 2-Me-4-OMe TG permeates through the cellular membranes, the intracellular decay times only varied slightly with respect to the decay time at the lowest phosphate concentration. The minor variations were most likely due to the medium tonicity. In the permeabilized CHO-k1 (α-toxin-treated) cells, the 2-Me-4-OMe TG decay time was dependent on the phosphate concentration at phosphate concentrations up to approximately 150 mM, which is within the physiological range. Figure S-3 of the SI shows the FLIM images from both α-toxin-treated and untreated CHO-k1 cells incubated in PBS at pH 7.35 and at various phosphate buffer concentrations ranging from 10 to 160 mM after applying an arbitrary color scale. Although the range of phosphate concentrations is narrow, the use of a color scale permits a fairly accurate observation of the different phosphate concentrations inside the permeabilized cells.

In Figure S-2 of the SI, we evaluated the difference in the decay time with respect to the decay time at the lowest phosphate buffer concentration because the absolute decay time values inside the cells (both α-toxin-treated and untreated cells) were larger than the values predicted for the free dye in solution. To investigate the cause of the increase in the 2-Me-4-OMe TG decay time inside CHO-k1 cells, we recorded fluorescence decay traces from the dye in aqueous solution in the presence of different concentrations of bovine serum albumin (BSA) as a crowding agent. We chose BSA as a crowding agent instead of polysaccharides such as Ficoll 400 because we recently demonstrated that Ficoll generates an association complex with the xanthenic dyes.[29] We collected the decay traces of 5×10^{-7} M 2-Me-4-OMe TG in aqueous 100 mM phosphate buffer at pH 7.35 with increasing BSA concentrations from 1 to 10 mg/mL. These fluorescence traces were tail-fitted as before with a time cutoff of 1.5 ns after the exciting pulse to eliminate the light scattered from the BSA. Interestingly, the fluorescence decay time of the dye increased with respect to the time in the absence of BSA by approximately 0.35 ns and remained constant at approximately 4.1 ns (see Figure S-4 of the SI). The results are consistent with the results from the dye in the cellular cytoplasm in which the crowded medium protects the dye from aqueous solvent

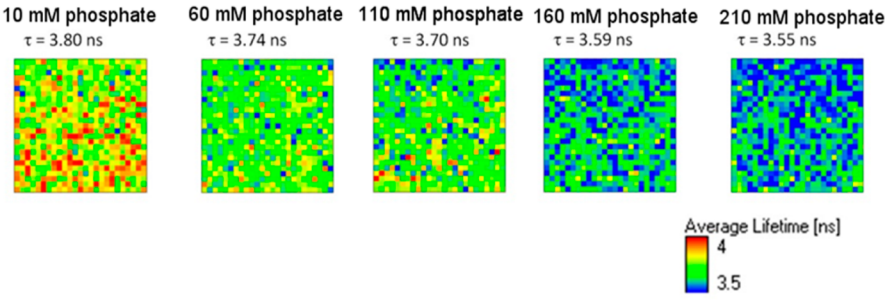

Figure 2. FLIM images from 2-Me-4-OMe TG (1×10^{-7} M) in commercial DMEM with different total phosphate concentrations at pH 7.35.

dx.doi.org/10.1021/jp405041c | J. Phys. Chem. B 2013, 117, 8143−8149

quenching. However, no decay time assignable as a result of interactions between the dye and the protein was observed.

Another series of experiments was performed with MC3T3-E1 preosteoblast cells treated with α-toxin and various concentrations of pH 7.35 phosphate buffers. The recovered FLIM images in Figure 3A show that 2-Me-4-OMe TG is

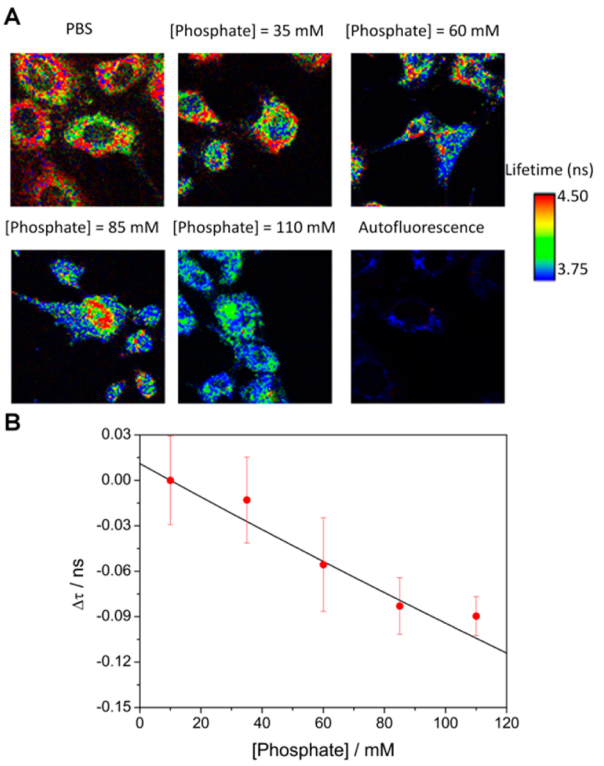

Figure 3. (A) FLIM images of 1×10^{-7} M 2-Me-4-OMe TG dye in osteoblast cells treated with α-toxin in PBS medium at different phosphate concentrations. The image labeled as autofluorescence corresponds to the FLIM image of the cells collected without the dye. (B) Changes in the decay time of the dye in osteoblast cells treated with α-toxin in PBS spiked with different phosphate concentrations. The τ decrease was calculated with reference to the decay time recovered in PBS solution (10 mM phosphate). The solid line represents the change in the decay times calculated using the rate constant values estimated by GCA.

sensitive to phosphate inside the osteoblast cytoplasm similar to the permeabilized CHO-k1 cells. Therefore, the decay time of the 2-Me-4-OMe TG dye is sensitive to the presence of phosphate in the cellular interior regardless of the cell type. Figure 3B shows the changes in the decay time of the dye inside the MC3T3-E1 osteoblast cells treated with α-toxin versus the spiked phosphate concentration. The solid line represents the change in the decay time predicted by the rate constant values estimated by the global compartmental analysis. The theoretical and experimental values exhibited an excellent agreement, which allowed the concentration of phosphate to be calculated inside the cell with remarkable accuracy.

After we demonstrated that 2-Me-4-OMe TG could be used to quantify the intracellular concentration of phosphate, we tested the usefulness of the FLIM 2-Me-4-OMe TG assay in a biological system with phosphate transport. Previously, we obtained FLIM images from the dye to know how the fluorophore enters the cell. The homogeneous distribution of the dye in the cytoplasm suggests that the penetration was via poration and that there was no formation of vacuoles that could change the local environment of the dye. The ability of osteoblasts to transport extracellular phosphate into the cell through a transporter has been established.[8] The MC3T3-E1 murine preosteoblast cell line is a well-established model for osteoblast differentiation.[25] Treatment of these cells with ascorbic acid (AA) and beta-glycerol phosphate (βGP) for 2 to 3 weeks results in extensive phosphate mineralization.[30,31] Early in the differentiation process, as the cells become dense and exit the cell cycle, a collagen matrix is formed in response to AA, and the level of the membrane-bound enzyme alkaline phosphatase (ALP) increases and peaks between days 7 and 14 generating inorganic phosphate from βGP.[25] Because the increase in the intracellular concentration of inorganic phosphate is the key signal that initiates mineralization in osteoblastic MC3T3-E1 cells,[25] increasing the concentration of phosphate from 1 to 3 mM reduces the premineralization period from 2 weeks to 2 days.[32] We used our FLIM methodology to evaluate the time evolution of intracellular phosphate intake from the extracellular media using the MC3T3-E1 cell line in which the expression of specific phosphate transporters is induced from the beginning of the differentiation process.[33]

MC3T3-E1 preosteoblast cells were cultured and differentiated to osteoblasts by incubating the cells in a differentiation medium containing βGP and AA to induce rapid mineralization. The cells were assayed at several stages of differentiation, and the results were compared with the results obtained using the nonpermeabilized CHO-k1 cells, which lack this phosphate transport system, as a control. Although complete mineralization of the osteoblast requires 21 days, the calcium phosphate that precipitates in the differentiation process cannot be detected by this FLIM methodology because of the insolubility of the compound in the cellular matrix. Therefore, short differentiation periods (up to 48 h) were selected to study phosphate transport.

Figure 4 shows that the 2-Me-4-OMe TG decay time inside CHO-k1 cells was insensitive to the incubation time indicating that phosphate ions were present in the extracellular media but did not permeate through the CHO-k1 cellular membrane. The 2-Me-4-OMe TG decay time inside the MC3T3-E1 cells

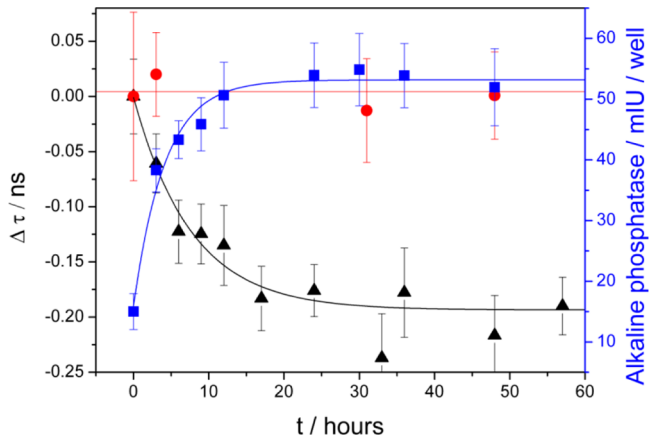

Figure 4. Changes in the 2-Me-4-OMe TG decay time in CHO-k1 (red circles) and osteoblastic MC3T3-E1 cells (black triangles) at different cellular differentiation times. Blue squares represent the extracellular levels of ALP during the differentiation of MC3T3-E1 cells. The solid lines are included as a visual reference.

dx.doi.org/10.1021/jp405041c | J. Phys. Chem. B 2013, 117, 8143−8149

decreased as the cellular differentiation of the preosteoblast line proceeded as shown in Figure 4. These results are expected because phosphate anions are readily transported through the cellular membrane of the osteoblasts and accumulate inside the cell until the phosphate precipitates around the nucleus after reaching a maximum concentration. These results are consistent with the morphology of the MC3T3-E1 cells, which exhibit a well-developed Golgi apparatus containing calcium phosphate precipitates.[25] As a control, we also investigated the extracellular levels of ALP in the differentiation process of the MC3T3-E1 cells because of the correlation between the extracellular activity of ALP and the increased intracellular inorganic phosphate content. Thus, in the differentiation process, the level of ALP in the extracellular medium should increase along with the concentration of phosphate inside the cell.[8] As shown in Figure 4, increased ALP was associated with a decrease in the 2-Me-4-OMe TG decay time as expected in the beginning of mineralization in osteoblastic MC3T3-E1 cells.[8]

Figure 5 shows exemplary FLIM images from 2-Me-4-OMe TG in CHO-k1 (A) and MC3T3-E1 osteoblast cells (B) at several differentiation times. Although the range of decay times is narrow, the use of a color scale allows a fairly accurate observation of the phosphate concentration inside the MC3T3-E1 cells and its changes with differentiation time. By contrast, the FLIM images from 2-Me-4-OMe TG inside CHO-k1 cells demonstrated that the decay was unaffected, which corresponded to a negligible intracellular phosphate concentration.

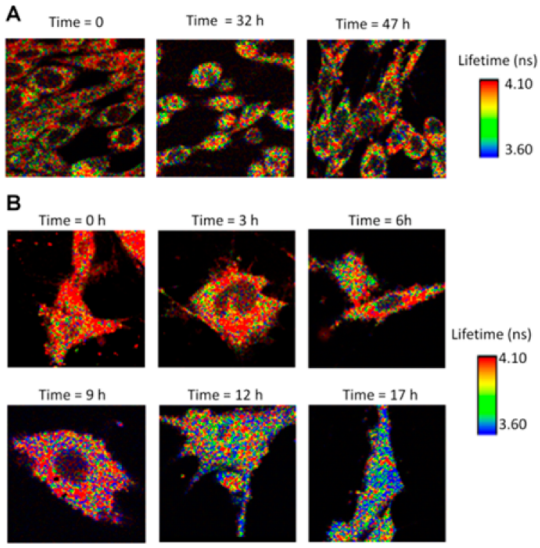

Figure 5. FLIM images of (A) 2-Me-4-OMe TG in CHO-k1 cells and (B) MC3T3-E1 preosteoblast cells in PBS medium, βGP, and AA at different differentiation times. In both panels, the 2-Me-4-OMe TG concentration in the medium was 1×10^{-7} M.

The recovered decay times shown in Figure 4 were fitted to exponential models to visualize the kinetics of phosphate penetration in the cellular cytoplasm. The data fitted well to a monoexponential model allowing to recover an apparent first-order kinetic rate constant of $3.1 \pm 0.7 \times 10^{-5}$ s^{-1} ($R^2 = 0.91$). The new methodology developed in this study can be used to quantify the rate of phosphate transport through the membrane of cells that have an active transport mechanism for that anion. Thus, this methodology would allow the evaluation of the bioavailability of different formulations containing phosphate anion. Of course, more studies are in progress to increase the sensitivity of the method as well as to keep the dye inside the cellular cytoplasm.

CONCLUSIONS

On the basis of the ESPT reaction of the 2-Me-4-OMe TG dye in the presence of phosphate and the rapid incorporation of the dye into the cells, we measured the changes in the intracellular phosphate concentration using FLIM. By using two different cell lines, CHO-k1 and osteoblastic MC3T3-E1, permeabilized with α-toxin, we observed an excellent agreement between the fluorescence decay time from the intracellular dye and the extracellular concentration of phosphate. Therefore, we tested the ability of the assay to evaluate the transport of extracellular phosphate into preosteoblasts during osteoblast differentiation. The new methodology here developed has allowed the recovery of the apparent kinetic rate constant of phosphate transport across the cellular membrane during osteoblast differentiation. Our results also showed that the intracellular levels of phosphate, as evidenced by the decrease in the decay time of the dye, correlated well with the extracellular activity of alkaline phosphatase. CHO-k1 cells, which lack the phosphate transport system, were employed as a negative control.

An important point for the accurate intracellular determination of the phosphate concentration using the methodology proposed herein lies on the parallel quantification of the intracellular pH. Because the total proton concentration affects the relative proportion of the monohydrogenphosphate and dihydrogen phosphate, the pH value also has an effect on the 2-Me-4-OMe TG fluorescence decay times. Therefore, although the external medium in the experiments related in Figure 3 is phosphate buffer at pH 7.35, it would be interesting to perform a simultaneous determination of the intracellular levels of phosphate and the pH value. The FLIM methodology can be easily extended to realize multiplexed determination by a dual-channel detection system.[34] By adding, for instance, pH-sensitive nanoparticles[35] emitting on a different spectral region as well as the 2-Me-4-OMe TG phosphate sensor, one could carry out multiplexed pH and phosphate quantification just by introducing appropriate dichroic mirrors and filters to the instrumentation.[34] Work in this subject is currently being performed in our research group.

ASSOCIATED CONTENT

Supporting Information

Scheme S-1 and Figures S-1 to S-4. This material is available free of charge via the Internet at http://pubs.acs.org.

AUTHOR INFORMATION

Corresponding Author

*E-mail: jalvarez@ugr.es.

Notes

The authors declare no competing financial interest.

ACKNOWLEDGMENTS

This work was supported by grants CTQ2010-20507/BQU from the Ministerio Español de Ciencia e Innovación (cofinanced by FEDER funds) and Fundación Marcelino Botín (awarded to R.S.).

REFERENCES

(1) Lakowicz, J. R. *Principles of Fluorescence Spectroscopy*, 3rd ed.; Springer: New York, 2006.

(2) Hötzer, B.; Ivanov, R.; Brumbarova, T.; Bauer, P.; Jung, G. Visualization of Cu^{2+} Uptake and Release in Plant Cells by Fluorescence Lifetime Imaging Microscopy. *FEBS J.* **2012**, *279*, 410−419.

(3) Kuimova, M. K.; Yahioglu, G.; Levitt, J. A.; Suhling, K. Molecular Rotor Measures Viscosity of Live Cells via Fluorescence Lifetime Imaging. *J. Am. Chem. Soc.* **2008**, *130*, 6672−6673.

(4) Okabe, K.; Inada, N.; Gota, C.; Harada, Y.; Funatsu, T.; Uchiyama, S. Intracellular Temperature Mapping with a Fluorescent Polymeric Thermometer and Fluorescence Lifetime Imaging Microscopy. *Nat. Commun.* **2012**, *3*, 705.

(5) Berezin, M. Y.; Achilefu, S. Fluorescence Lifetime Measurements and Biological Imaging. *Chem. Rev.* **2010**, *110* (5), 2641−2684.

(6) Schenk, T.; Apples, N. M. G. M.; van Elswijk, D. A.; Irth, H.; Tjaden, U. R.; van der Greef, J. A Generic Assay for Phosphate-Consuming or -Releasing Enzymes Coupled On-Line to Liquid Chromatography for Lead Finding in Natural Products. *Anal. Biochem.* **2003**, *316*, 118−126.

(7) Hirose, J.; Fujiwara, H.; Magarifuchi, T.; Iguti, Y.; Iwamoto, H.; Kominami, S.; Hiromi, K. Copper Binding Selectivity of N- and C-sites in Serum (human)- and Ovo-Transferrin. *Biochim. Biophys. Acta* **1996**, *1296*, 103−111.

(8) Beck, G. R.; Zerler, B.; Moran, E. Phosphate is a Specific Signal for Induction of Osteopontin Gene Expression. *Proc. Natl. Acad. Sci. U.S.A.* **2000**, *97*, 8352−8357.

(9) Kim, S. K.; Lee, D. H.; Hong, J.-I.; Yoon, J. Chemosensors for Pyrophosphate. *Acc. Chem. Res.* **2009**, *42* (1), 23−31.

(10) Ito, M.; Haito, S.; Furumoto, M.; Uehata, Y.; Sakurai, A.; Segawa, H.; Tatsumi, S.; Kuwahata, M.; Miyamoto, K. Unique Uptake and Efflux Systems of Inorganic Phosphate in Osteoclast-Like Cells. *Am. J. Physiol. Cell Physiol.* **2007**, *292*, C526−C534.

(11) Ganjali, M.; Hosseini, M.; Memari, Z.; Faridbod, F.; Norouzi, P.; Goldooz, H.; Badiei, A. Selective Recognition of Monohydrogen Phosphate by Fluorescence Enhancement of a New Cerium Complex. *Anal. Chim. Acta* **2011**, *708* (1−2), 107−110.

(12) Yguerabide, J.; Talavera, E. M.; Alvarez-Pez, J. M.; Quintero, B. Steady-State Fluorescence Method for Evaluating Excited State Proton Reactions: Application to Fluorescein. *Photochem. Photobiol.* **1994**, *60*, 435−441.

(13) Alvarez-Pez, J. M.; Ballesteros, L.; Talavera, E.; Yguerabide, J. Fluorescein Excited-State Proton Exchange Reactions: Nanosecond Emission Kinetics and Correlation with Steady-State Fluorescence Intensity. *J. Phys. Chem. A* **2001**, *105* (26), 6320−6332.

(14) Boens, N.; Basaric, N.; Novikov, E.; Crovetto, L.; Orte, A.; Talavera, E. M.; Alvarez-Pez, J. M. Identifiability of the Model of the Intermolecular Excited-State Proton Exchange Reaction in the Presence of pH Buffer. *J. Phys. Chem. A* **2004**, *108* (40), 8180−8189.

(15) Crovetto, L.; Orte, A.; Talavera, E. M.; Alvarez-Pez, J. M.; Cotlet, M.; Thielemans, J.; De Schryver, F. C.; Boens, N. Global Compartmental Analysis of the Excited-State Reaction between Fluorescein and (±)-*N*-Acetyl Aspartic Acid. *J. Phys. Chem. B* **2004**, *108* (19), 6082−6092.

(16) Orte, A.; Bermejo, R.; Talavera, E. M.; Crovetto, L.; Alvarez-Pez, J. M. 2′,7′-Difluorofluorescein Excited-State Proton Reactions: Correlation between Time-Resolved Emission and Steady-State Fluorescence Intensity. *J. Phys. Chem. A* **2005**, *109* (12), 2840−2846.

(17) Paredes, J. M.; Garzon, A.; Crovetto, L.; Orte, A.; Lopez, S. G.; Alvarez-Pez, J. M. Effects of the Anion Salt Nature on the Rate Constants of the Aqueous Proton Exchange Reactions. *Phys. Chem. Chem. Phys.* **2012**, *14* (16), 5795−5800.

(18) Boens, N.; Qin, W.; Basaric, N.; Orte, A.; Talavera, E. M.; Alvarez-Pez, J. M. Photophysics of the Fluorescent pH Indicator BCECF. *J. Phys. Chem. A* **2006**, *110* (30), 9334−9343.

(19) Orte, A.; Crovetto, L.; Talavera, E. M.; Boens, N.; Alvarez-Pez, J. M. Absorption and Emission Study of 2′,7′-Difluorofluorescein and Its Excited-State Buffer-Mediated Proton Exchange Reactions. *J. Phys. Chem. A* **2005**, *109* (5), 734−747.

(20) Böhmer, M.; Wahl, M.; Rahn, H. J.; Erdmann, R.; Enderlein, J. Time-Resolved Fluorescence Correlation Spectroscopy. *Chem. Phys. Lett.* **2002**, *353*, 439−445.

(21) Widengren, J.; Kudryavtsev, V.; Antonik, M.; Berger, S.; Gerken, M.; Seidel, C. A. M. Single-Molecule Detection and Identification of Multiple Species by Multiparameter Fluorescence Detection. *Anal. Chem.* **2006**, *78* (6), 2039−2050.

(22) Crovetto, L.; Paredes, J. M.; Rios, R.; Talavera, E. M.; Alvarez-Pez, J. M. Photophysics of a Xanthenic Derivative Dye Useful as an "On/Off" Fluorescence Probe. *J. Phys. Chem. A* **2007**, *111* (51), 13311−13320.

(23) Paredes, J. M.; Crovetto, L.; Rios, R.; Orte, A.; Alvarez-Pez, J. M.; Talavera, E. M. Tuned Lifetime, at the Ensemble and Single Molecule Level, of a Xanthenic Fluorescent Dye by Means of a Buffer-Mediated Excited-State Proton Exchange Reaction. *Phys. Chem. Chem. Phys.* **2009**, *11* (26), 5400−5407.

(24) Urano, Y.; Kamiya, M.; Kanda, K.; Ueno, T.; Hirose, K.; Nagano, T. Evolution of Fluorescein as a Platform for Finely Tunable Fluorescence Probes. *J. Am. Chem. Soc.* **2005**, *127* (13), 4888−4894.

(25) Sudo, H.; Kodama, H.; Amagi, Y.; Yamamoto, S.; Kasai, S. In Vitro Differentiation and Calcification in a New Clonal Osteogenic Cell Line Derived from Newborn Mouse Calvaria. *J. Cell Biol.* **1983**, *96*, 191−198.

(26) Giron, M. D.; Havel, C. M.; Watson, J. A. Mevalonate-Mediated Suppression of 3-hydroxy-3-methylglutaryl Coenzyme A Reductase Function in Alpha-Toxin-Perforated Cells. *Proc. Natl. Acad. Sci. U.S.A.* **1994**, *91*, 6398−6402.

(27) Braslavsky, S. E. Glossary of Terms Used in Photochemistry, 3rd Edition. *Pure Appl. Chem.* **2007**, *79*, 293−465.

(28) Maus, M.; Cotlet, M.; Hofkens, J.; Gensch, T.; De Schryver, F. C.; Schaffer, J.; Seidel, C. A. M. An Experimental Comparison of the Maximum Likelihood Estimation and Nonlinear Least-Squares Fluorescence Lifetime Analysis of Single Molecules. *Anal. Chem.* **2001**, *73* (9), 2078−2086.

(29) Paredes, J. M.; Crovetto, L.; Orte, A.; Lopez, S. G.; Talavera, E. M.; Alvarez-Pez, J. M. Photophysics of the Interaction between a Fluorescein Derivative and Ficoll. *J. Phys. Chem. A* **2011**, *115* (46), 13242−13250.

(30) Franceschi, R. T.; Iyer, B. S.; Cui, Y. Effects of Ascorbic Acid on Collagen Matrix Formation and Osteoblast Differentiation in Murine MC3T3-E1 Cells. *J. Bone Miner. Res.* **1994**, *9*, 843−854.

(31) Quarles, D.; Yohay, D. A.; Lever, L. W.; Caton, R.; Wenstrup, R. J. Distinct Proliferative and Differentiated Stages of Murine MC3T3-E1 Cells in Culture: An in Vitro Model of Osteoblast Development. *J. Bone Miner. Res.* **1992**, *7*, 683−692.

(32) Wang, D.; Christensen, K.; Chawala, K.; Xiao, G.; Krebsbach, P. H.; Franceschi, R. T. Isolation and Characterization of MC3T3-E1 Preosteoblast Subclones with Distinct in Vitro and in Vivo Differentiation/Mineralization Potential. *J. Bone Miner. Res.* **1999**, *14*, 893−903.

(33) Suzuki, A.; Ghayor, C.; Guicheux, J.; Magne, D.; Quillard, S.; Kakita, A.; Ono, Y.; Miura, Y.; Oiso, Y.; Itoh, M.; Caverzasio, J. Enhanced Expression of the Inorganic Phosphate Transporter Pit-1 Is Involved in BMP-2-Induced Matrix Mineralization in Osteoblast-Like Cells. *J. Bone Miner. Res.* **2006**, *21*, 674−683.

(34) Abbasi, A. Z.; Amin, F.; Niebling, T.; Friede, S.; Ochs, M.; Carregal-Romero, S.; Montenegro, J.-M.; Rivera Gil, P.; Heimbrodt, W.; Parak, W. J. How Colloidal Nanoparticles Could Facilitate Multiplexed Measurements of Different Analytes with Analyte-Sensitive Organic Fluorophores. *ACS Nano* **2011**, *5* (1), 21−25.

(35) Ruedas-Rama, M. J.; Orte, A.; Hall, E. A. H.; Alvarez-Pez, J. M.; Talavera, E. M. Quantum Dot Photoluminescence Lifetime-Based pH Nanosensor. *Chem. Commun.* **2011**, *47*, 2898−2900.